V European Conference on Computational Fluid Dynamics
ECCOMAS CFD 2010
J. C. F. Pereira and A. Sequeira (Eds)
Lisbon, Portugal, 14–17 June 2010

DEVELOPMENT OF 1D PERFORMANCE ANALYSIS TOOL FOR A MICROTURBINE RADIAL COMPRESSOR USING CFD

A. Javed, M. Olivero, and J.P. van Buijtenen

Process and Energy Department
Delft University of Technology
Leeghwaterstraat 44, 2628 CA Delft, The Netherlands
E-mail: a.javed@tudelft.nl, m.olivero@tudelft.nl, j.p.vanbuijtenen@tudelft.nl

Key words: Microturbine, Radial Compressor, 1D Performance Prediction Tool, Computational Fluid Dynamics, Two-Zone Flow, Secondary Flow Analysis

Abstract. *Gasturbine part manufacturers are often not involved in the design process. This means opportunities to optimize the design process including issues, such as manufacturing costs, are missed. This paper presents the development of performance modeling tools that would help in optimizing the design of microturbine radial compressors from the manufacturer's perspective. The methodology predicts performance by sequentially calculating the processes in the impeller, diffuser and the scroll. This multistation, meanline performance model applies not only the basic fluid dynamic principles but also the two-zone flow model and a foundation of empirical information to predict the compressor characteristics realistically. The vaneless diffuser analysis has been carried out through numerical integration of one-dimensional (1D) flow equations, which allowed studying the steady motion of a compressible flow with friction effects and area change. A technique for simple overhung scrolls based on geometric area ratio has been included to conclude the comprehensive performance modeling. Due to lack of information about the complex flow structure in such impellers, an aerodynamic analysis has been performed using Computational Fluid Dynamics (CFD) with an emphasis on the two-zone flow characteristics. An important correlation for the secondary mass flow and area fractions has been developed and utilized to improve the performance prediction capability of the 1D model. Validation of the model and aerodynamic analysis has been carried out by comparing the results with the experimental data. The model is useful in predicting the effects of geometrical changes of compressor components on performance and therefore presents a valuable tool for optimizing the designs, including manufacturing issues.*

NOMENCLATURE

A	Area	$\dot{m}$	Mass Flow
C_P	Pressure Recovery Coefficient	N	Rotational speed
DR	Diffusion Ratio	p	Pressure
LE	Leading Edge	R	Gas Constant
M	Mach Number	T	Temperature

TE	Trailing Edge
W	Relative velocity
γ	Specific Heat Ratio
ε	Secondary Flow Area Fraction
η	Efficiency/Effectiveness
σ	Entropy Gain Function
χ	Secondary Flow Mass Fraction

Subscript

0	Stagnation State
1	Impeller Inlet
2	Impeller Outlet
geo	Geometric
p	Primary Flow
s	Secondary Flow
t	Tip

Superscript

‘	Relative Condition

1 INTRODUCTION

1.1 Background

There are two prime stakeholders in the gasturbine industry which are involved in product design and development: Original Equipment Manufacturer (OEM) and the OEM subsystem suppliers. OEM is mainly responsible for the product design and development whereas the subsystem supplier contributes in specific parts production, having a limited influence on the product design itself. Being the designer of gasturbine components that have been optimized to achieve high performance, the OEM is often unable to realize the manufacturing limitations of the subsystem supplier. On the contrary, although having state of the art manufacturing facilities, the subsystem suppliers are unable to process the required dimensions and tolerance levels and therefore, they request the OEM for dimensional relaxations. Undoubtedly a lack of communication exists and has to be inspected.

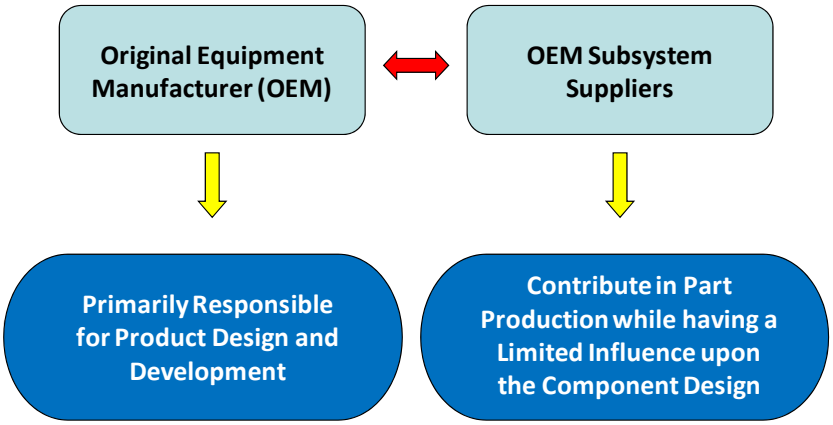

Figure 1: Gasturbine industry stakeholders

Emphasis on the design for performance will continue, but would likely be considered a foundation or threshold rather than the central requirement as typified in the past decades. In the future, it is very likely that life, weight, size, cost, assembly complexity and other parameters might be continuously monitored while the design process goes forward. This will surely change the character of advance designs and facilitate the multidisciplinary design process of the near future.

From the above discussion we find a strong relationship between manufacturing aspects and costs with the performance of the gasturbine components. Aim of the

current study is to analyze the effects of small changes in the component design variables on overall engine performance and design simplicity for cost-effective manufacturing. The possibility of judging the influence of parts design on engine performance and manufacturing costs will help the Dutch gasturbine industry to optimize their production technology process and develop indigenous design capabilities to communicate effectively with the OEM.

1.2 The microturbine test case

A recuperated microturbine for Combined Heat and Power (CHP) generation is under development at Micro Turbine Technology BV (MTT). It produces a power output of 3 kWe to be used for domestic purposes as micro CHP units and auxiliary power units/parking heaters for trucks. The microturbine is fitted with a radial compressor comprising an impeller, a vaneless diffuser and a discharge volute. Experimental data for the microturbine has been provided by MTT. The geometric data is shown in Table 1.

Impeller	
Inducer Tip Radius	12.8 mm
Inducer Hub Radius	4.75 mm
Discharge Radius	17.5 mm
Discharge Width	2.6 mm
Number of Blades	12 (6 Full, 6 Splitter)
Inducer Blade Tip Angle	-64^0
Backsweep Angle	-34^0
Vaneless Diffuser	
Discharge Radius	32.3 mm
Discharge Width	1.7 mm
Volute	
Discharge Diameter	27.6 mm

Table 1: Microturbine radial compressor stage specifications

Microturbines are fairly unique in a sense that simple scaling of a high performance large gasturbine will not result in a good microturbine because of a large change in Reynolds number, heat transfer between hot and cold components and geometrical restrictions related to material and manufacturing of miniaturized components [1]. Thus the microturbine is an interesting study case for achieving good performance while maintaining a cost effective production as it is proposed to be produced in large numbers.

1.3 Performance modeling tool

In this paper a methodology to develop a performance analysis tool for a microturbine radial compressor has been presented. The core idea behind developing such a model is to generate performance maps with minimum amount of input in form of basic geometric data and operating conditions. The model has been programmed into a computer code with MATLAB®. It is based on the “level 3 design approach” in which various components constituting a radial compressor have been modeled separately [2]. Geometric data for the components are known and by using the model, the performance of the compressor stage is analyzed and summarized in a performance map.

1.4 Requirements from CFD

Information related to the flow structure in microturbines is insufficient resulting in the performance prediction process to be troublesome. The performance model involves the two-zone flow phenomena and therefore, to cater the deficiency of available information, CFD has been used. The idea is to use CFD in order to simulate the compressor stage at design and off-design operating conditions. The analysis has provided valuable information related to the secondary flow generation that eventually affects the microturbine performance. This information has been used effectively to improve the performance prediction capability of the 1D model. Validation of the performance model and the aerodynamic analysis has been carried out by comparing the results with the microturbine experimental data. After validation, the numerical results can be trusted and used for improving the prediction capability of the performance model under development, particularly for microturbines.

2 1D PERFORMANCE ANALYSIS TOOL

A clear distinction between design and analysis mode is important at this stage. In a design process, a geometric configuration is created to meet certain performance specifications set by the customer. On the other hand, in the analysis mode, one attempts to predict the performance of a configuration based on its known or proposed dimensions. In order to have a complete set of design tools, it is necessary both to generate geometric configurations and to predict the performance of the resulting geometric configurations over a wide range of possible operating conditions. Such tools can be used effectively in establishing optimized configurations.

The current model is based on the level 3 design approach in which various components constituting a radial compressor have been modeled separately [2]. Geometric data for the components is known and given in Table 1. The stage performance modeling scheme is illustrated in Fig 2.

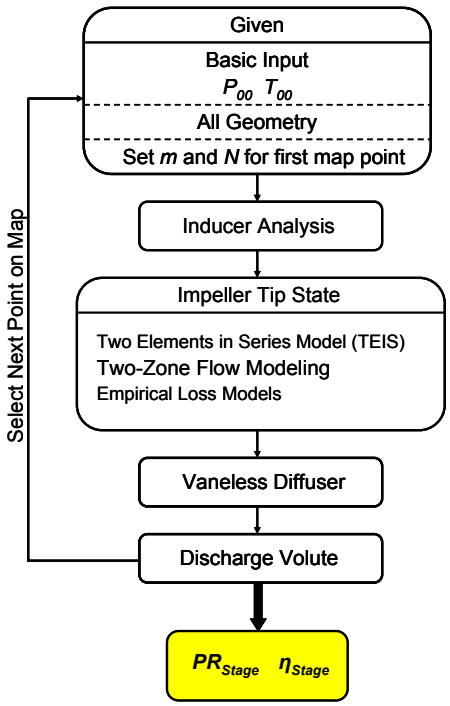

Figure 2: Level 3 design analysis scheme

Any procedure to model the flow process through the compressor impeller, or any other component, must provide an adequate description of the essential phenomena involved [3]. Whether the model is adequate can only be assessed against suitable experimental data. A complete set of equations has been used for the performance modeling [2, 3]. Since the test case is a microturbine radial compressor, some tuning is required in the empirical data to achieve a reasonable agreement between the model results and experimental results.

2.1 Impeller performance modeling

The impeller is responsible for the energy transfer to the fluid. It consists essentially of two components: the inducer and the exducer where the energy is imparted to the fluid by the centrifugal forces. The flow enters the impeller in the axial direction and leaves in the radial. The blades should be designed to eliminate large decelerations or accelerations of the flow in the impeller, leading to high losses and flow separation.

2.1.1 Inducer modeling

The function of an inducer is to increase the angular momentum of the fluid without increasing its radius of rotation. For the inducer design analysis, the following parameters should be known:

1. Inlet stagnation pressure and temperature.
2. Degree of pre-whirl.
3. Mass flow rate of the working fluid.

For the current study, standard atmospheric conditions have been set in the code to compare the results with the experimental data. No pre-whirl has been considered for the analysis and Mach number of the flow entering the inducer has been predicted through an iterative procedure. A blockage factor of 2% and an axial velocity ratio parameter of 1.02 for ideal simple axial inlet have been used [2].

2.1.2 Diffusion prediction

Experimental data concerning diffusion in the impeller passage were not available and therefore some pragmatic method had to be used for estimating the pressure rise across the radial passage. The Two Elements in Series (TEIS) model has been used [2]. The impeller passage is considered to be a rotating diffuser while recognizing the importance of conventional diffuser parameters such as area ratio and length to width ratio for each stream tube. In the TEIS model, the first element, which can either be a diffuser or nozzle in character, feeds the second element, which is most often a diffuser. In order to relate the exit conditions of the impeller to appropriate inlet conditions, the diffusion ratio or Mach number ratio parameter may be employed. A very simple analytical model has been written for these two elements where the diffusion ratio is given as

$$DR = \frac{1}{1-\eta_a C_{pa,i}} \times \frac{1}{1-\eta_b C_{pb,i}}. \quad (1)$$

The effectiveness parameters for the inlet portion η_a and the passage η_b have been set to 0.5 and 0.3 respectively and gave a reasonable estimation [2]. Together they form an important set of parameters which control the amount of diffusion in the impeller

passage. Once *DR* is estimated, the primary flow velocity W_{2p} at the impeller exit has been calculated using the following relation:

$$DR = \frac{W_{1t}}{W_{2p}}, \tag{2}$$

where W_{1t} is the inducer tip relative velocity and has been used since the inducer tip is the most heavily loaded and influences the diffusion process in the impeller primarily.

2.1.3 Two-zone flow modeling

Radial compressor fluid dynamics is probably the most complicated array of fluid processes routinely encountered by man in his engineering [4]. The flow field emerging inside a radial compressor passage is very complex, three-dimensional, and turbulent all under the influence of curvature (due to curved and swept blades) and rotation [5]. Turbulence structure in these curved and rotating passages is affected by rotation and curvature, thus invalidating the models developed for stationary, non-curved two-dimensional flows. Although this complex flow structure was observed quite early in the 20th century, it was not completely understood until Eckardt's famous work was published [6]. It gave a thorough insight to the two-zone flow phenomenon originating from the three-dimensional boundary layers, secondary flows and flow separations [6]. Figure 3 illustrates the two-zone flow structure inside an impeller passage.

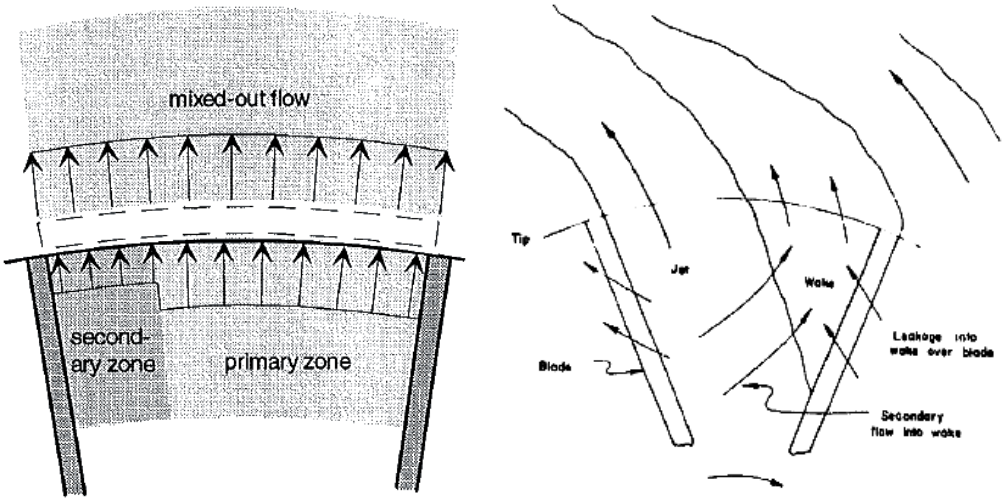

Figure 3: Two-zone flow structure in an impeller [2, 4]

Considering these complications, radial compressor design and analysis have relied heavily on empirical correlations. The TEIS model described in Section 2.1.2 provides an estimation of the primary flow velocity W_{2p}. The flow in the primary zone is considered to be isentropic in nature, while all the irreversibility is assumed to be carried by the secondary zone flow. The work transfer in an adiabatic impeller is related to both the change in total enthalpy across it and the change in the whirl speed defined by the Euler turbomachinery equation. Conservation of rothalpy between the inlet and the outlet states determines the static temperature T_{2p} leading to the calculation of the static pressure p_{2p}. Since both primary and secondary flows surround the entire impeller passage, an iterative method has been used to predict the flow distribution between the

two zones. Introduction of secondary flow mass fraction χ and secondary flow area fraction ε is necessary at this stage:

$$\chi = \frac{\dot{m}_s}{\dot{m}} \ , \tag{3}$$

$$\varepsilon = \frac{A_s}{A_{geo}} . \tag{4}$$

These parameters can be considered as the core of the two-zone modeling process as they define the division of mass and area between the primary and secondary flows. Figure 4 shows two different data sets of data: one is for the three Eckardt's impellers having large diameters while the other set for nine comparatively smaller impellers [2].

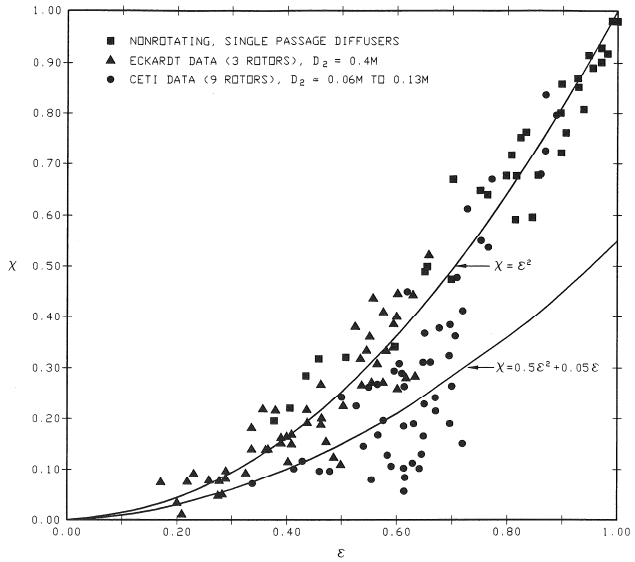

Figure 4: Secondary flow mass vs. area fraction [2]

Since the algorithm has been developed to be used for small compressors, correlation representing the CETI impellers was considered initially for the model.

$$\chi = 0.5\varepsilon^2 + 0.05\varepsilon . \tag{5}$$

The correlation was found to be inappropriate for the test case compressor after an early analysis and therefore, an alternative had to be devised. For the model, all the entropy generated within the impeller by shear and leakage is assumed to appear in the secondary zone. The secondary zone losses contribute to the overall impeller loss when the secondary flow mixes with the primary flow downstream of the impeller tip. The main assumptions applied to the secondary zone are:

1. Fluid is perfectly guided by the blades.
2. Primary and secondary flow static pressures are equal.
3. Front cover friction is negligible.

For an adiabatic process, entropy is a measure of the degree of irreversibility or deviation from the ideal process. This finds clear expression in the enthalpy-entropy diagram. Hence it is logical to seek solutions based on the entropy change of the actual process as compared with an isentropic process between similar end states. The "Entropy Gain" approach [3] is a very convenient and compact means to express the non-isentropic character of real processes and is expressed as

$$\sigma = \exp\left(-\Delta s / R\right) = \left[\frac{T_{2p}}{T'_{02s}}\left(1+\frac{\gamma-1}{2}M'^{2}_{2s}\right)\right]^{\frac{\gamma}{\gamma-1}}. \quad (6)$$

A new technique has been introduced in the modeling procedure. The impeller loss production has been determined using various empirical loss correlations available in the literature [7]. These loss correlations predict the incidence, blade loading, skin friction and clearance losses while the mixing loss is calculated by the pressure difference across the mixing region. This method is different from a more general entropy gain approach for two-zone flow modeling in which the impeller losses are predicted as a bulk using Eq. 6.

The energy dissipated at the mixed-out state as the fluid flows has been calculated through the application of 1D energy, momentum and continuity equations presented [3]. At the mixed-out discharge state of the impeller, effects of rear face disk friction, recirculation and leakage have been considered and are termed as external or parasitic losses. Calculation of mixed-out state and two sets of equations for primary and secondary flow present a complete description of the impeller flow. Computing the mixing process is important as it provides closure to the system of equations and determines some very important parameter concerning the impeller flow field.

2.2 Diffuser and scroll 1D performance modeling

The pinched vaneless diffuser has been analyzed by means of 1D flow equations [8]. They represent a 1D model to study the steady motion of a compressible flow, with wall friction effects and area change. Neither the effects of the mixing losses due to non-uniform flow conditions at the diffuser inlet nor heat transfer are considered. The variations of the fluid properties are determined by a succession of states through the diffuser, as a function of the radius for a prescribed variation of the diffuser effective height.

A simple overhung type scroll is being used for the current test case radial compressor stage. A fairly reasonable modeling technique [2] for the simple overhung scroll has been used in the present model.

3 NUMERICAL ANALYSIS SETUP

3.1 Requirement

In Section 2.1.3, Eq. 5 is initially used for 1D performance modeling. The correlation represents the two-zone flow development for CETI impellers (Fig. 4), which are larger in size than the microturbine compressor analyzed here. Thus the correlation is unable to comply for predicting a reasonable performance. As the two-zone flow model is a significant part of the code, a new correlation is required which would satisfy the test case microturbine compressor flow structure. Since CFD has developed into a potential tool for turbomachinery analysis, it has been used effectively in the current study.

3.2 CFD Tools

ANSYS CFX 12.0 [10] has been used for the study. It is a commercial CFD code which solves 3D compressible Reynolds averaged Navier-Stokes equations in stationary or rotating frames of reference using a finite volume discretization method. It uses a range of turbulent models with both logarithmic wall function and two-layer approaches to model the boundary layer.

A 3D geometric model of the radial compressor stage has been used in ANSYS BladeGen 12.0 [11], ANSYS TurboGrid 12.0 [12] and GAMBIT 2.4.6 [13]. BladeGen acts as a medium in which complex turbomachinery geometries can be simplified and transformed into useful blade geometry profile and curves. These are imported into TurboGrid which is a very quick and easy to use grid generator. GAMBIT is another useful grid generator but does not specialize in turbomachinery grids. These tools have been used to create a simplified geometry and mesh as they allow a rapid 3D screening and analysis of turbomachinery components. Mesh generation, boundary condition specification and design changes become greatly simplified and automated.

3.3 Grid Generation

For the current study, a single passage impeller and diffuser configuration has been simulated using periodic boundary conditions. The volute has not been included in the domain to simplify the problem. The impeller has been modeled in BladeGen using data from the 3D geometric model and exported to TurboGrid for grid generation. A 3D structured grid has been developed using the H-Grid and O-Grid topologies. The O-Grid provides a good mesh around the blades while rest of the passage consists of H-Grid. The grid sensitivity analysis in [9] showed a grid of 0.15 million elements to be sufficient but for improving mesh resolution, a fine mesh comprising of 0.25 million elements has been used. A 2% tip clearance has been introduced with five elements in the clearance gap. Such percentage is reasonable as the tip clearance generally lays between 1-3% of blade trailing edge height at design speed operations. The dimensionless near-wall distance y^+ has been set to 1 in order to resolve the boundary layer.

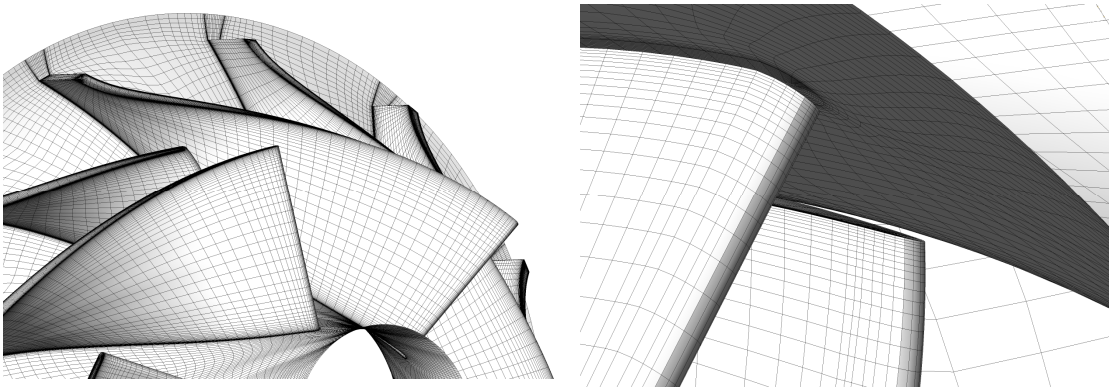

(a) (b)

Figure 5: 3D structured mesh: (a) impeller (b) 2% clearance gap

The diffuser has been modeled in GAMBIT 2.4.6, a pre-processor tool used for grid generation. A structured grid comprising of around 0.08 million elements with a well resolved near-wall mesh has been created.

3.4 Boundary Conditions and Solver

The impeller and diffuser domains and their respective boundary conditions are shown in Fig. 6. Ambient conditions have been defined at the inlet, allowing the CFD results to be compared with the experimental data. To simulate various operating conditions, the outlet boundary condition has been specified different mass flows at a particular rotational speed. Rotational periodic boundary conditions have been set up since single passage configuration has been used. The impeller shroud has been defined

as counter-rotating that allows the relative motion between the rotating impeller and the stationary shroud to be captured.

The interface between the impeller and diffuser has been defined as 'Frozen Rotor'. In this approach, the frame of reference is changed but the relative motion of the components across the interface remains fixed. This allows the components to have a fixed relative position throughout the calculations. Frozen rotor model produces a steady-state solution to the multiple frames of reference problems and requires much lower amount of computational effort than the transient approaches. The lack of capability in capturing the transient effects at the interface and losses as the flow is mixed between the stationary and rotating components is a disadvantage though.

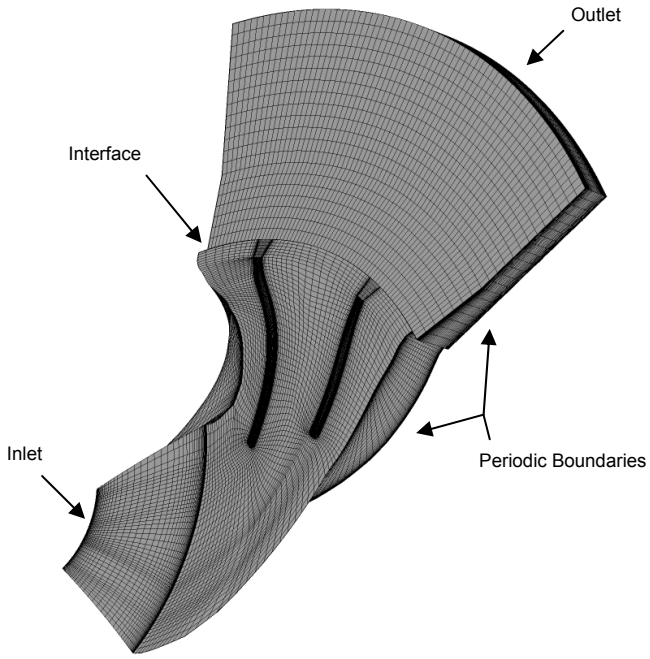

Figure 6: Impeller and diffuser domains with respective boundary conditions

Explicit Algebraic Reynolds Stress Model (EARSM) coupled with Baseline (BSL) k-ω has been used as the turbulent solver [10]. The model has been derived from the Reynolds stress transport equations and gives a nonlinear relation between the Reynolds stresses and the mean strain-rate and vorticity tensors. Due to higher order terms many flow phenomena are included in the model without the need to solve transport equations. The BSL-EARSM model captures the consequences of secondary flows and flows with streamline curvature and system rotation effectively. Automatic near-wall treatment switches from wall-functions to a low Reynolds number near-wall formulation as the mesh is refined. High-resolution advection scheme has been set for the solution of model equations. The convergence criteria have been set to $1x10^{-5}$ for the residuals while isentropic compression efficiency has been monitored for assessing the solution convergence or stabilization.

4 CFD PERFORMANCE PREDICTION

4.1 Validation

The numerical simulations are performed at rotational speeds of 220 krpm and 190 krpm for which the experimental data was available. Maintaining a constant speed, the simulations are performed at various mass flow rates to generate a performance map.

The results have been compared with the available experimental data for validation (Fig. 7). The CFD simulations predict the performance reasonably well. Since only impeller and the diffuser have been simulated, the volute section has been analyzed using the 1D model in order to complete the stage performance prediction and compare the numerical data with the experimental ones.

It is noted from Fig. 7 that the performance trend is followed by the computed results computed data and is encouraging for the next stage. Some level of discrepancy is found however, the uncertainty of the experimental data as well as the limitations of the frozen rotor approach and of the turbulence model, especially for part load conditions, must be taken into account. The tip-clearance is another significant issue which has to be studied properly in order to quantify the effects of leakage flows through clearance gaps.

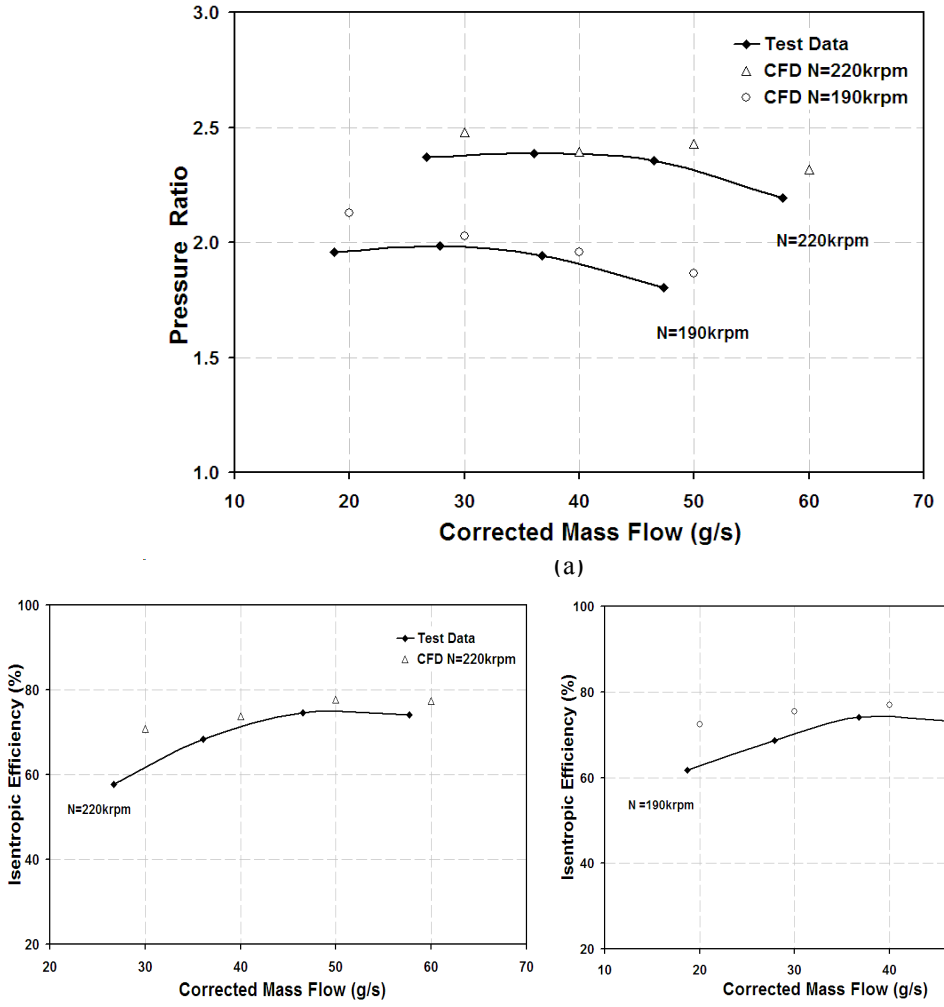

Figure 7: Validation of the CFD results: (a) pressure ratio (b) isentropic efficiency

4.2 Secondary flow analysis

The results from the numerical analysis have been used to understand the flow behavior in the impeller. The aim is to determine the secondary flow properties and find out the relationship between the secondary flow mass and area fractions. This analysis has been used to improve the performance prediction capability of the 1D model.

The relative velocity and its components (meridional, tangential and to some extent the radial) have been used to study the secondary flow in the impeller. The Meridional

velocity represents the mass flow rate in the passage and therefore meridional velocity contours and charts have been created to capture the secondary mass flow. A surface has been created in the ANSYS CFX post-processor near the trailing edge of the blades. Three data lines (near hub, mid-span and the shroud) have been created at the same location. Figure 8 shows the meridional velocity profile at the blade trailing edge for N=220krpm and the different mass flow rates.

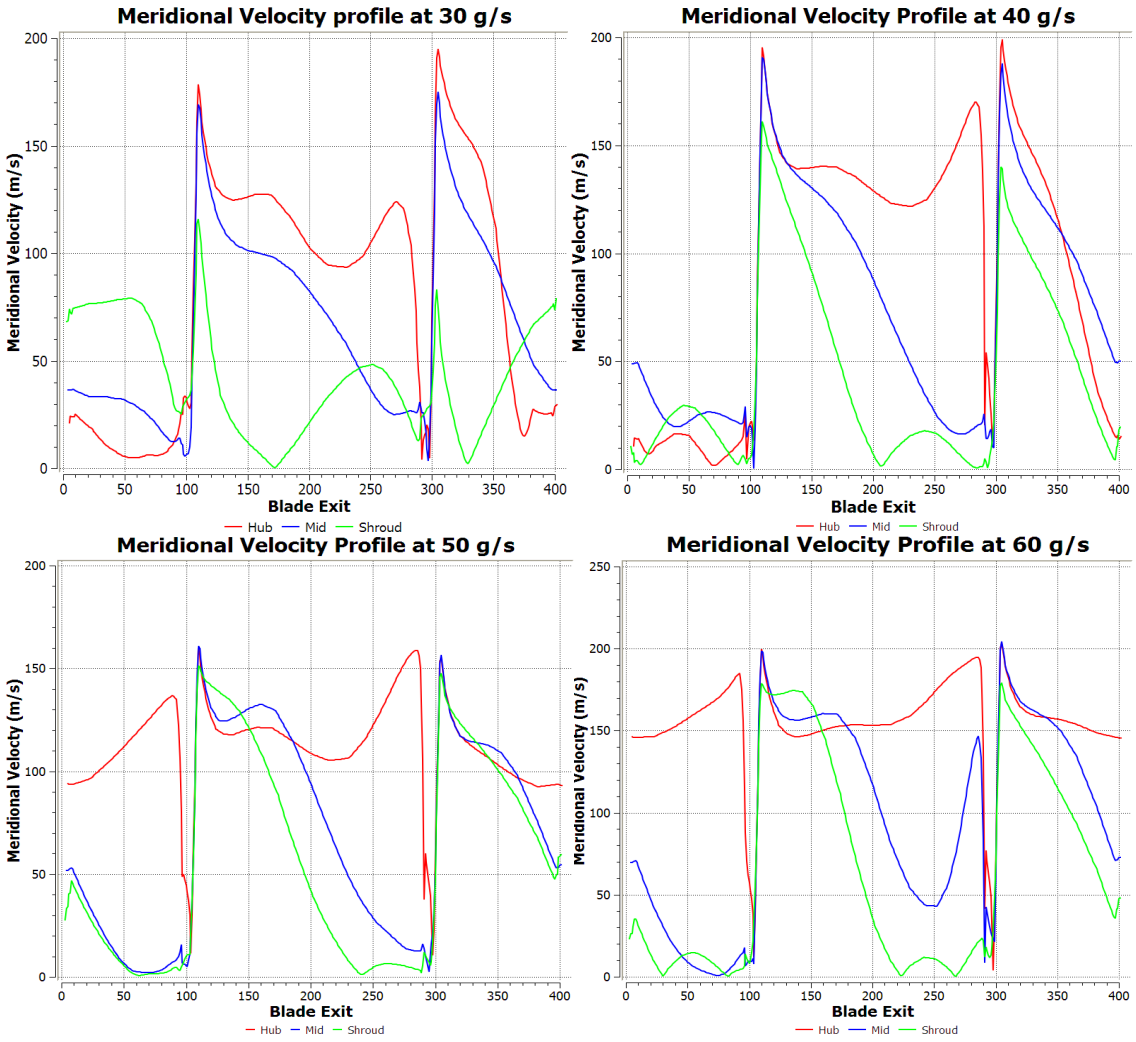

Figure 8: Meridional velocity profiles at blade TE for N= 220krpm

Similar plots are created for N=190krpm, but not shown here due to lack of space. It is evident from Fig. 8 that the flow pattern is influenced by the varying mass flow rate at a particular rotational speed. Such behavior can also be seen in the meridional velocity contour plots shown in Fig. 9. The low velocity regions in the figures signify the secondary flow and it can be seen that the secondary zone increases as the mass flow is reduced from 60 g/s to 30 g/s. The hub is the least effected region as compared to mid-span and near-shroud.

Meridional velocities below 50 m/s have been assumed to be representing the secondary flow. To calculate the mass flow through this region, averaged meridional velocities have been calculated in the span-wise direction. By using mass-averaged densities and the approximated area covered by the low meridional velocities at the blade trailing edge, the secondary mass flow has been computed.

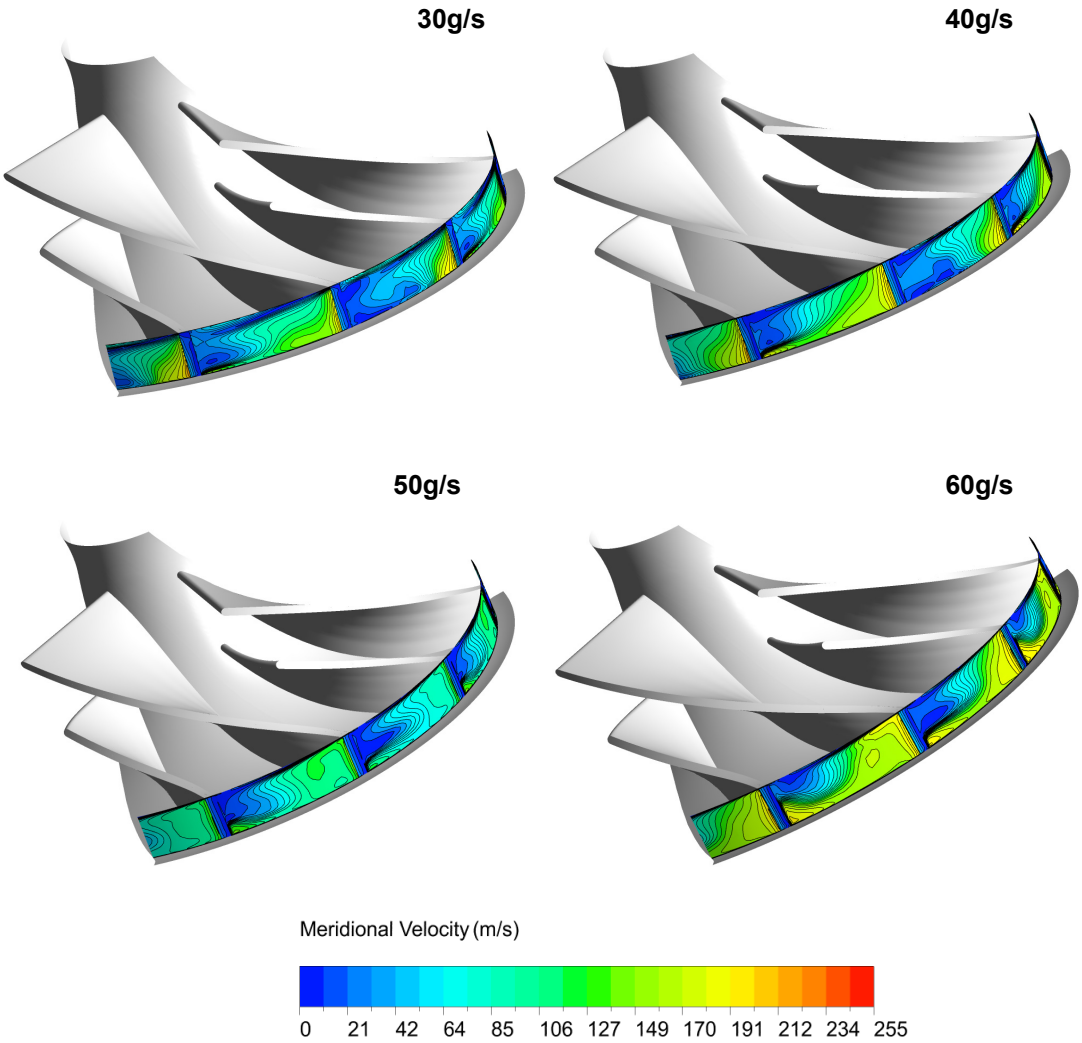

Figure 9: Meridional velocity contours at blade TE for N= 220krpm

As the mass flow through the secondary flow is determined, it is necessary to predict the area it occupies at the impeller exit. Relative velocity contours at the impeller outlet and streamlines in the impeller passage shown in Fig. 10 represent the extent of passage area covered by the secondary flow. It can be seen that the secondary flow is more vigorous at low mass flow rates due to increased flow separation increased leakage. Thus the surrounded area is larger than as compared to what is observed at higher mass flow rates. At design operating condition, the secondary flow region appears close to the shroud while rest of the passage allows the primary flow to pass through. As the mass flow is reduced, due to increased separation and leakage, the secondary flow grows in span-wise direction thus reaching the hub. Even though the tip-clearance is as low as 2% of blade tailing edge height, the clearance gap has been observed to be actively involved in the secondary flow generation process. The leakage flow passing through the clearance gap is found to be flowing backwards due to increased back pressure in the impeller indicating a possible stall. Therefore, it can be concluded that the tip-clearance issue becomes quite significant for radial compressors particularly in case of a microturbine.

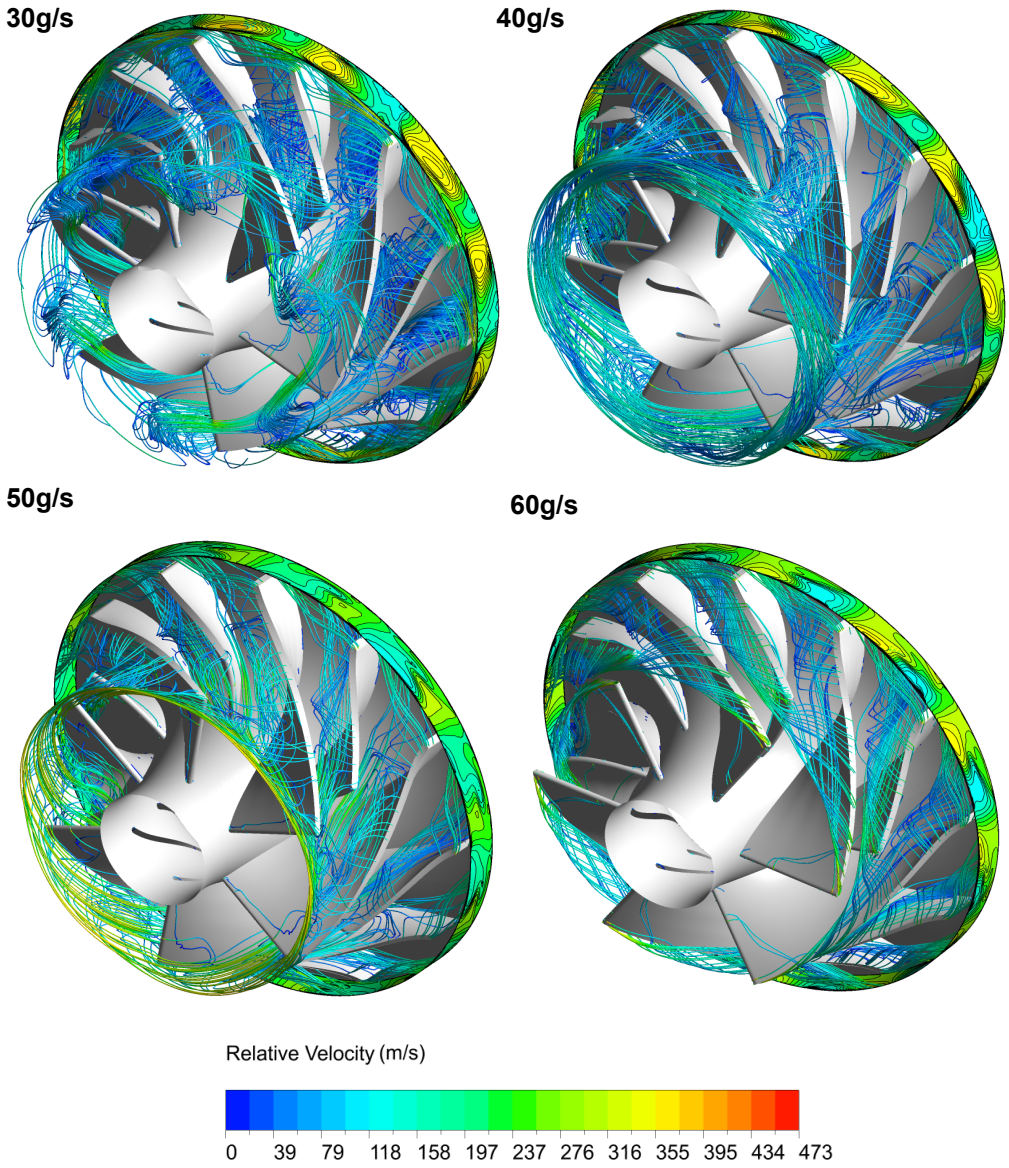

Figure: 10 Relative velocity streamlines for N= 220krpm

The full and splitter blades control the passage flow differently as observed Fig. 9 and Fig. 10. Since the splitter is located almost half way between the impeller inlet and exit, the secondary flow originating from the full blade leading edge also impacts the splitter blade. Near the shroud, the secondary flow from the full blade travels to the splitter blade suction side and merges with its secondary flow thus increasing the vortex size. Such an influence is even stronger at low mass flow rates as the impeller operates near to stall.

Figure 11 illustrates the secondary flow development at various stream-wise locations from leading to trailing edge of the blades. Flow separation is observed near the shroud at 30% streamwise location. As the flow proceeds through the passage, leakage flow crossing into the suction side through the clearance gap mixes with the separated flow to create the secondary flow vortex. The flow properties at the blade trailing edge are important for the study since the 1D performance model predicts the end state properties and is not concerned with the flow development in the passage.

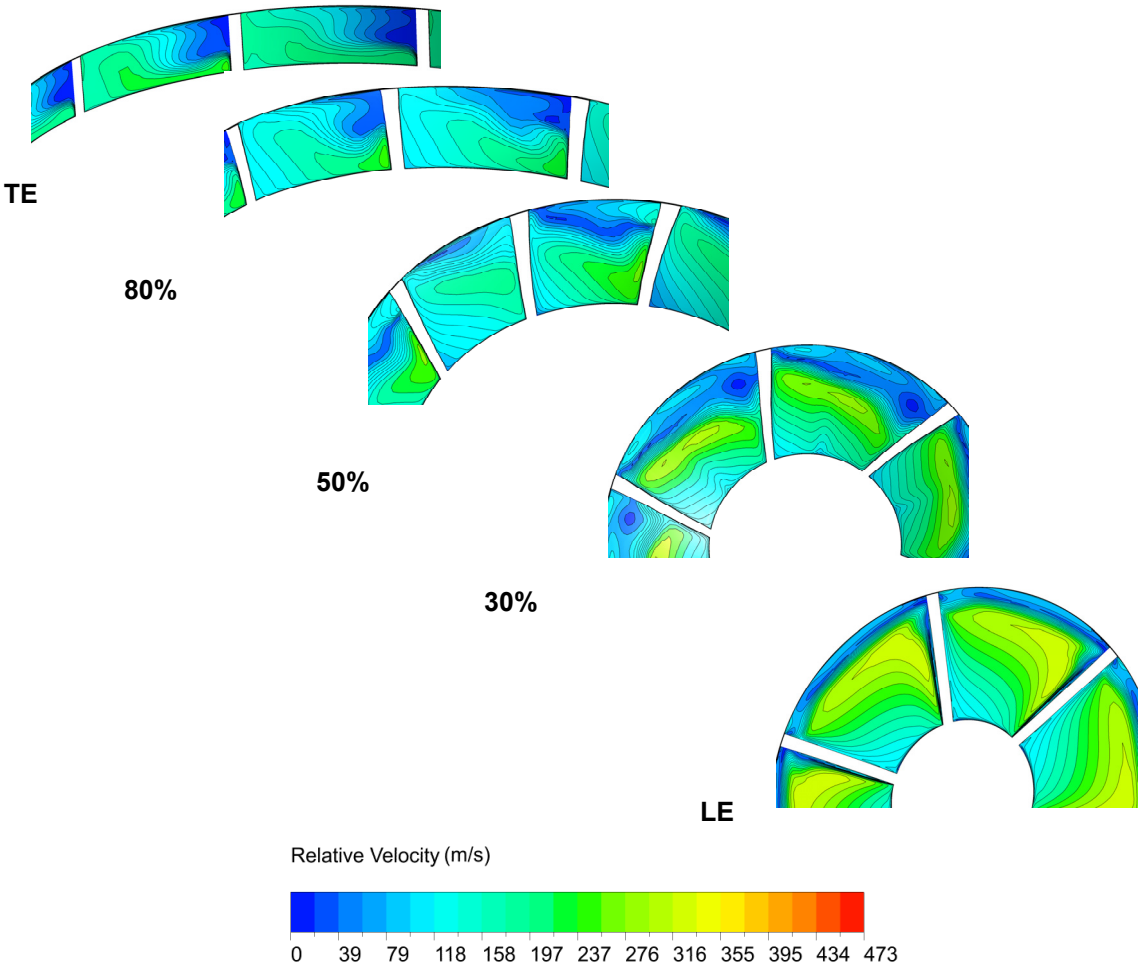

Figure 11: Secondary flow at various streamwise locations for 50 g/s and N= 220krpm

The required information concerning the secondary flow mass and area fractions is now available and has been plotted in Fig. 12 for the two speed lines and their respective mass flow rates. From the figure, it has been seen that at low mass flow rate, around 80% of impeller exit area is covered with the secondary flow. A trend line that relates the secondary flow mass and area fraction has been extrapolated from the data.

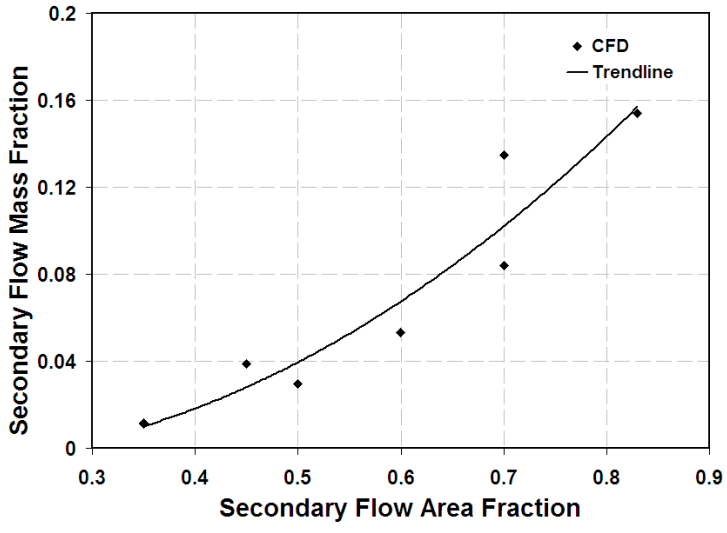

Figure 12: Secondary flow mass and area fractions

Using the plot a new correlation has been developed which is intended to satisfy the two-zone flow structure in the test case microturbine impeller.

$$\chi = 0.3337\varepsilon^2 + 0.0877\varepsilon \,. \tag{7}$$

Equation 7 is significant and unique for the two-zone flow modeling as it represents the flow behavior in the microturbine radial compressor and corresponds to its distinct flow characteristics.

5 1D MODEL PERFORMANCE PREDICTION

Equation 5 representing the CETI impellers is now replaced with Eq. 7 in the 1D performance analysis code. The model has been used to generate the compressor performance map which is shown in Fig. 13. It can be observed from the comparative study that the new correlation has performed up to expectations and is a significant step forward. It can be concluded that the 1D model predicts the compressor performance reasonably well with the new correlation representing the flow characteristics for the particular test case microturbine radial compressor.

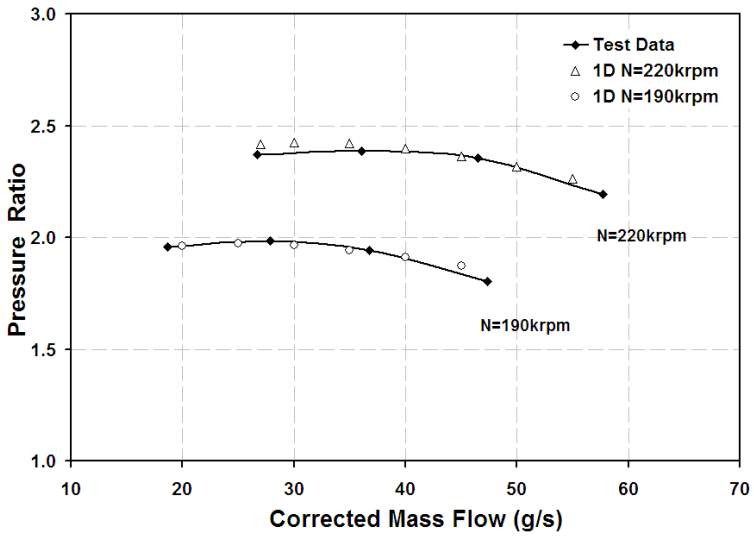

(a)

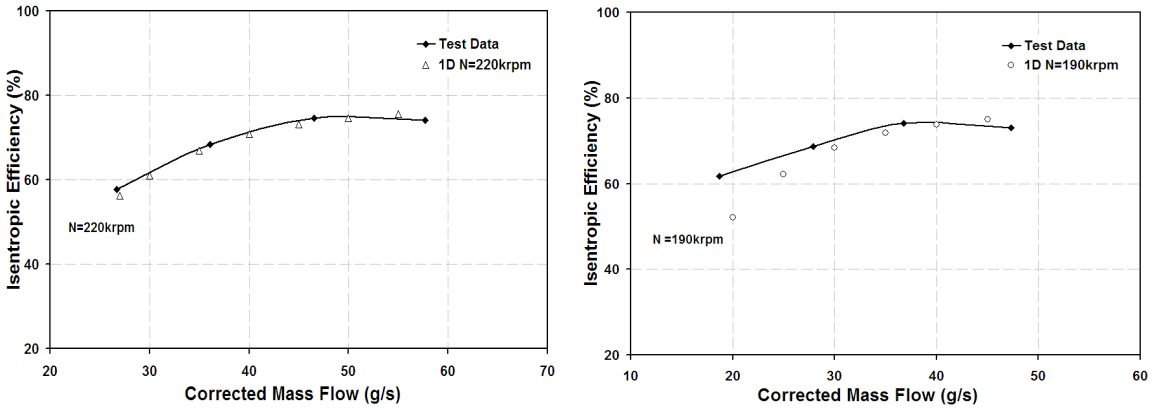

(b)

Figure 13: 1D model compressor maps; (a) pressure ratio (b) isentropic efficiency

6 CONCLUSIONS

A 1D performance model has been developed for a microturbine radial compressor stage using two-zone flow modeling techniques and various empirical loss models. The model is required to analyze performance effects due to small geometric changes with an aim to achieve a simplified design at reduced manufacturing complexities for developing of such components. The results have been validated against the experimental data. The comparison shows a reasonable accuracy and therefore the CFD outcomes can be better trusted for this particular application. Meridional velocity has been used to determine the secondary mass flow in the impeller. The area covered by the secondary flow has been approximated using the relative velocity streamlines.

The following can be concluded:

- An equation which links the primary and secondary flow in the microturbine impeller has been developed using CFD. It has been used effectively in the 1D performance model. The model predicts the performance of the microturbine radial compressor satisfactorily (Fig. 13).
- It has been found that the secondary flow dominates the impeller passage as the mass flow is reduced to near stall regions.
- Backflow has also been observed at low mass flow rate operations with leakage flow supporting the secondary flow development (Fig. 10).
- Tip clearance affects are significant for microturbines as 80% of passage area has been found surrounded by secondary flow with a contribution from the clearance gap (Fig. 10 and Fig. 11).
- The numerical method performs well for studying secondary flows.

REFERENCES

[1] R. Van den Braembussche, Micro Gas Turbines – A Short Survey of Design Problems, *Educational Notes RTO-EN-AVT-131*, Paper nº 1 (2005)

[2] D. Japikse, Centrifugal Compressor Design and Performance, *Concepts ETI, Inc.*, Wilder, USA (1996)

[3] A. Whitfield and N.C. Baines, Design of Radial Turbomachines, *Longman Scientific & Technical*, Essex, England (1990)

[4] R.C. Dean, The Fluid Dynamic Design of Advanced Centrifugal Compressors, *Lecture Series of the Von Karman Institute*, Brussels, Belgium (1974)

[5] B. Lakshminarayana, Fluid Dynamics and Heat Transfer of Turbomachinery, *John Wiley & Sons, Inc.*, New York, USA (1996)

[6] D. Eckardt, Instantaneous Measurements in the Jet-Wake Discharge Flow of a Centrifugal Compressor Impeller, *Journal of Engineering for Power*, **97**, 337-346 (1975)

[7] H.W. Oh, E.S. Yoon and M.K. Chung, An Optimum Set of Loss Models for Performance Prediction of Centrifugal Compressors, *Proceedings of the Institution of Mechanical Engineers, Part A: Journal of Power and Energy*, **211**, 331-338 (1997)

[8] J.D. Stanitz, One-Dimensional Compressible Flow In Vaneless Diffusers Of Radial And Mixed Flow Centrifugal Compressors Including Effects Of Friction, Heat Transfer And Area Change, *National Advisory Committee for Aeronautics*, Paper nº TN 2610 (1952)

[9] M. Olivero, A. Javed and J.P. van Buijtenen, Aerodynamic Analysis Of A Micro Turbine Centrifugal Compressor, *Proceeding of the ASME Turbo Expo 2010*, Glasgow, Scotland, Paper nº GT2010-23112 (2010)

[10] ANSYS CFX, Release 12.0 Documentation, *ANSYS, Inc.*, Canonsburg, USA (2009)

[11] ANSYS TurboGrid, Release 12.0 Documentation, *ANSYS, Inc.*, Canonsburg, USA (2009)

[12] ANSYS BladeGen, Release 12.0 User' Guide, *ANSYS, Inc.*, Canonsburg, USA (2009)

[13] GAMBIT 2.4 User's Guide, *Fluent, Inc.*, Lebanon, USA (2007)